Cell Reports

Report

Identification of and Molecular Basis for SIRT6 Loss-of-Function Point Mutations in Cancer

Graphical Abstract

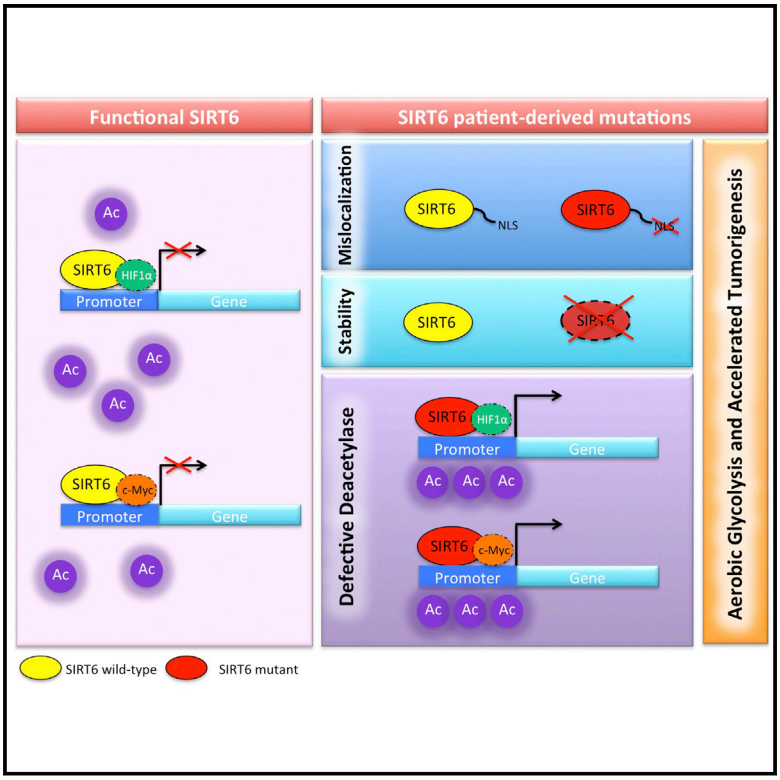

Authors

Sita Kugel, Jessica L. Feldman, Mark A. Klein, ..., Gad Getz, John M. Denu, Raul Mostoslavsky

Correspondence

jmdenu@wisc.edu (J.M.D.), rmostoslavsky@mgh.harvard.edu (R.M.)

In Brief

Kugel et al. identified eight naturally occurring tumor-associated point mutations in SIRT6 that alter stability, localization, or enzymatic activity. Based on biochemical, biological, and structural analyses, these mutations render SIRT6 unable to repress transformation. These mutations demonstrate that SIRT6 deacetylase activity, not demyristoylase activity, is critical for SIRT6 tumor-suppressor functions.

Highlights

- Eight loss-of-function SIRT6 mutations were identified in human cancers
- SIRT6 mutants alter either SIRT6 stability, localization, or enzymatic activity
- SIRT6 mutants fail to repress glycolysis and cellular transformation
- Deacetylase, not demyristoylase, activity is critical for SIRT6 tumor-suppressor function

Kugel et al., 2015, Cell Reports *13*, 479–488
October 20, 2015
http://dx.doi.org/10.1016/j.celrep.2015.09.022

CellPress

Cell Reports
Report

Identification of and Molecular Basis for SIRT6 Loss-of-Function Point Mutations in Cancer

Sita Kugel,[1,7] Jessica L. Feldman,[4,7] Mark A. Klein,[4] Dafne M. Silberman,[6] Carlos Sebastián,[1] Craig Mermel,[1,3] Stephanie Dobersch,[5] Abbe R. Clark,[1] Gad Getz,[1,3] John M. Denu,[4,*] and Raul Mostoslavsky[1,2,3,*]
[1]The Massachusetts General Hospital Cancer Center, Harvard Medical School, Boston, MA 02114, USA
[2]The Center for Regenerative Medicine, The Massachusetts General Hospital, Boston, MA 02114, USA
[3]The Broad Institute of MIT and Harvard, Cambridge, MA 02142, USA
[4]The Department of Biomolecular Chemistry and the Wisconsin Institute for Discovery, University of Wisconsin, Madison, WI 53715, USA
[5]Max-Planck-Institute for Heart and Lung Research, Bad Nauheim 61231, Germany
[6]Center for Pharmacological and Botanical Studies (CEFYBO)-CONICET, Facultad de Medicina, UBA, Buenos Aires 1121, Argentina
[7]Co-first author
*Correspondence: jmdenu@wisc.edu (J.M.D.), rmostoslavsky@mgh.harvard.edu (R.M.)
http://dx.doi.org/10.1016/j.celrep.2015.09.022

SUMMARY

Chromatin factors have emerged as the most frequently dysregulated family of proteins in cancer. We have previously identified the histone deacetylase SIRT6 as a key tumor suppressor, yet whether point mutations are selected for in cancer remains unclear. In this manuscript, we characterized naturally occurring patient-derived SIRT6 mutations. Strikingly, all the mutations significantly affected either stability or catalytic activity of SIRT6, indicating that these mutations were selected for in these tumors. Further, the mutant proteins failed to rescue *sirt6* knockout (SIRT6 KO) cells, as measured by the levels of histone acetylation at glycolytic genes and their inability to rescue the tumorigenic potential of these cells. Notably, the main activity affected in the mutants was histone deacetylation rather than demyristoylation, pointing to the former as the main tumor-suppressive function for SIRT6. Our results identified cancer-associated point mutations in SIRT6, cementing its function as a tumor suppressor in human cancer.

INTRODUCTION

The (NAD)+-dependent histone deacetylase, SIRT6, is a mammalian sirtuin with broad functions including glucose homeostasis, maintenance of genome stability, and suppression of cellular transformation (Mostoslavsky et al., 2006; Sebastián et al., 2012; Zhong et al., 2010). In this context, SIRT6 co-represses both HIF1α and MYC by deacetylating histone 3 (H3) lysine 9 (K9) and lysine 56 (K56) at the promoters of several glycolytic and ribosomal protein genes. Consequently, SIRT6-deficient cells display increased glycolysis even under normoxic conditions, a phenomenon termed aerobic glycolysis by Otto Warburg, who first described this phenotype in cancer cells (Warburg, 1956). Indeed, SIRT6 inhibits cancer growth in a manner that depended on glycolytic metabolism (Sebastián et al., 2012). Importantly, we found SIRT6 commonly downregulated or deleted in human cancer, where lower SIRT6 expression is associated with poor prognosis. Thus, SIRT6 acts as a key tumor suppressor and critical node between cellular transformation and metabolism (Sebastián et al., 2012).

SIRT6-dependent phenotypes have been attributed to its intrinsic histone deacetylase activity, which seems negligible in biochemical assays, but can be enhanced by binding to nucleosomes and/or long-chain fatty acids (Feldman et al., 2013; Gil et al., 2013; Kawahara et al., 2009; Michishita et al., 2008; Sebastián et al., 2012; Zhong et al., 2010). Recent studies have shown that SIRT6 can also function as a protein demyristoylase (Feldman et al., 2013; Jiang et al., 2013), introducing the possibility that SIRT6 may suppress tumorigenesis through the deacylation of long-chain fatty acyl groups rather than histone deacetylation. The lack of known SIRT6 point mutations selected for in human cancer has hindered progress in the molecular understanding of the tumor-suppressive roles of SIRT6.

In this manuscript, we identify and characterize eight naturally occurring tumor-associated point mutations in SIRT6 that alter stability, localization, and/or enzymatic activity and characterize their ability to repress HIF1α and MYC transcriptional activity, glycolytic metabolism, and cellular transformation.

RESULTS

SIRT6 Is Mutated in a Variety of Human Cancers

In order to determine whether SIRT6 could be inactivated in human tumors through point mutations, we analyzed somatic mutations obtained via exome sequencing of patient-derived tumor samples from 12 tumor types in the TCGA and found eight somatic mutations in SIRT6. These mutations were found in a variety of tumor types such as non-small-cell lung cancer, renal clear cell carcinoma, cervical carcinoma, and melanoma (Figure 1A). Although SIRT6 did not meet statistical significance as a result of the low frequency of mutations (Lawrence et al., 2014; http://www.tumorportal.org), all of the mutations were

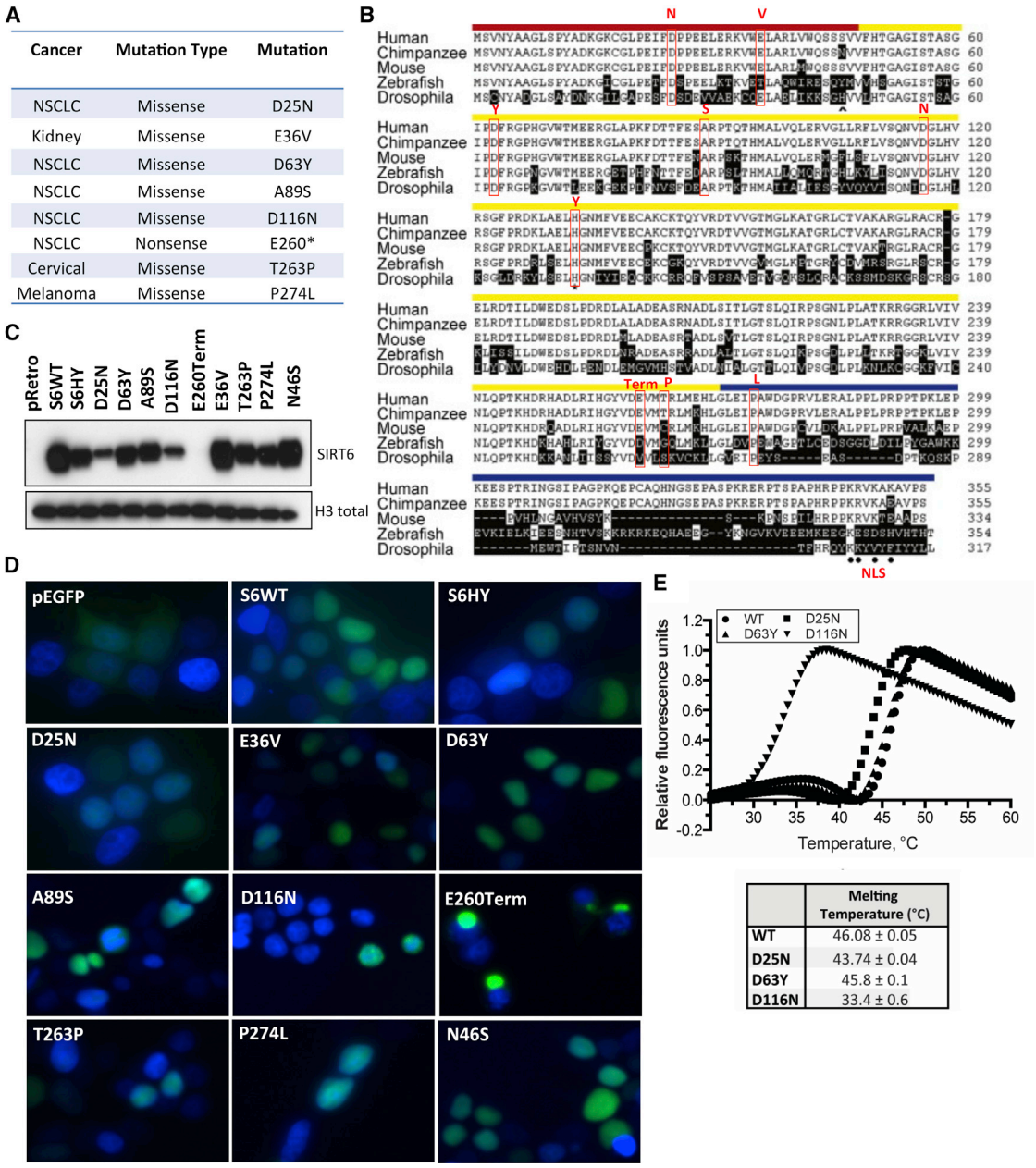

Figure 1. Identification of Patient-Derived SIRT6 Loss-of-Function Mutations in Cancer

(A) Table of patient-derived SIRT6 point mutations, the disease, type of mutation, and amino acid change.

(B) Alignment of metazoan SIRT6 homologs. Red boxes highlight the position of the mutations in the N terminus (red), catalytic core (yellow), or C terminus (blue).

(C) Western blot of chromatin fraction in SIRT6 KO MEFs with doxycycline-inducible overexpression of wild-type (WT) SIRT6 and SIRT6 mutants.

(D) Sub-cellular localization of WT and mutant SIRT6 proteins. Fluorescent images of fixed 293T cells transiently transfected with the indicated EGFP-tagged SIRT6 deletion and point mutants are shown. Nuclei are co-stained with DAPI (40×).

(E) Thermal denaturation assays were performed to determine the melting temperature (T_m) of WT (circle), D25N (square), D63Y (triangle), and D116N (upside-down triangle) SIRT6. A graph with representative experiments is shown. At least three trials were performed for each SIRT6 variant.

nonsynonymous; seven of them were missense mutations, and one mutation was a nonsense mutation, suggesting that they may have functional relevance. The mutations occurred throughout the protein and involved residues that are highly conserved from flies to humans (Figure 1B). Mutations occurring in the N terminus include an aspartic acid at position 25 mutated to asparagine (D25N) and a glutamic acid at position 36 mutated to valine (E36V). Catalytic domain mutations include an aspartic acid at position 63 mutated to tyrosine (D63Y), an alanine at position 89 mutated to serine (A89S), an aspartic acid at position

116 mutated to asparagine (D116N), a threonine at position 263 mutated to a proline (T263P), and finally a glutamic acid at position 260 replaced with a stop codon (E260Term), leading to premature truncation of the protein and loss of the C terminus and nuclear localization signal. Only one mutation involved the C terminus, where a proline at position 274 was mutated to a lysine (P274L) (Figures 1A and 1B).

SIRT6 Point Mutations that Alter Localization or Stability

Each of these SIRT6 mutations were cloned and expressed in *sirt6* knockout (SIRT6 KO) mouse embryonic fibroblasts (MEFs). We also included, as a control, a variant found in the human population, N46S. Three of the mutants (D25N, D116N, and E260Term) demonstrated reduced chromatin-bound and whole-cell lysate protein levels, despite equivalent mRNA expression, suggesting mislocalization or poor protein stability (Figures 1C, S1A, and S1B). We noted that the appearance of reduced expression with the D25N mutant may have been an artifact of reduced antibody affinity because the antibody epitope includes D25. Therefore, we used a GFP antibody to detect a GFP-tagged version of wild-type (WT) SIRT6 and each of the SIRT6 mutants to confirm that SIRT6 D25N expression and localization to chromatin was equivalent to WT (Figure S1C), whereas the D116N and E260Term mutants displayed reduced levels in chromatin, as observed with the non-GFP-tagged constructs (Figure 1C). We also noted that each of the mutant alleles localized to the nucleus, except for the E260Term mutant, consistent with the lack of a nuclear localization signal (Figure 1D). Interestingly, the levels of the D116N mutant were consistently reduced both in the chromatin fraction when expressed in mammalian cells and when recombinantly overexpressed in *E. coli,* suggesting defective protein stability. To test this hypothesis, we determined the melting temperature of D116N, D25N, D63Y, and WT SIRT6. Whereas D25N (43.74°C ± 0.04°C) and D63Y (45.8°C ± 0.1°C) exhibited melting temperatures very similar to WT (46.08°C ± 0.05°C), the melting temperature of D116N was ~13°C lower (33.4°C ± 0.6°C; Figure 1E). At physiologic temperatures, this protein is expected to be largely unfolded and subject to degradation.

In Silico Analysis Predicts Functionally Significant Structural Changes Induced by Cancer-Associated SIRT6 Mutations

To gain insight into the functional significance of these mutated residues, we analyzed the previously solved co-crystal structure of SIRT6 bound to ADP-ribose and an H3K9 myristoylated peptide (PDB: 3ZG6; Jiang et al., 2013; Figure 2A). Aspartic acid 25 is located in the N-terminal domain (NTD) and hydrogen bonds to the backbone amide nitrogen and carbonyl oxygen of H255 as well as to the ε-amino group of K33 (Figure 2B). The NTD is required for catalytic activity and chromatin association (Tennen et al., 2010); therefore, a mutation to asparagine will likely disrupt the orientation and interactions between the loop and the Rossmann-fold domain. Aspartic acid 63 is located in the NAD^+-binding pocket, ~3 Å from the adenosine moiety of NAD^+, and forms hydrogen-bonding interactions with amino acids in the active site (Figure 2C). Therefore, a mutation to tyrosine is predicted to have a highly detrimental effect on the ability of SIRT6 to bind NAD^+ and catalyze deacetylation. Alanine 89 and aspartic acid 116 are located on loops in the back of the active site (Figures 2D and 2E). Alanine 89 forms a backbone hydrogen bond interaction with T85, and mutation to serine might affect the orientation of this loop. The invariant aspartic acid residue (D116) forms a hydrogen bond to the carboxamide amino group of nicotinamide, and mutation to glutamine will disrupt this conserved interaction. Glutamic acid 36 and threonine 263 are located in the Rossmann-fold domain and form hydrogen bonds with R39 and D259, respectively (Figures 2F and 2G). Mutation of E36 to valine will abolish this hydrogen bond, which could destabilize other interactions in the helix. A proline mutation at T263 will disrupt the structure of the helix in the Rossmann-fold. Proline 274 is located in the proline-rich C-terminal domain (CTD) loop, and a mutation to threonine may affect the orientation of the loop (Figure 2H). Taken together, all of the identified mutations are likely to affect catalytic activity directly or through structural rearrangements.

Deacetylase Activity of SIRT6 Mutants

We next performed a highly sensitive, quantitative, in vitro deacetylase assay on purified recombinant SIRT6 mutants and compared the results obtained with WT enzyme. First, WT or SIRT6 mutants were reacted with 50 μM H3K9Ac peptide and 0.5 mM NAD^+. Reaction substrates and products were separated by HPLC and quantified. Strikingly, all mutants displayed decreased deacetylase activity relative to WT SIRT6 ($3.9 \pm 0.3 \times 10^{-4}$ μmol min^{-1} mg $SIRT6^{-1}$). D25N, E36V, A89S, T263P, and P274L all exhibited approximately 50% of WT SIRT6 activity, whereas D116N and D63Y yielded nearly negligible deacetylase activity at ~2% of WT SIRT6 levels (Figure 2I). Importantly, the non-cancer-associated N46S variant displayed deacetylase activity similar to WT. The decreased catalytic activity of D116N SIRT6 is due in part to decreased protein stability, as evidenced by its 13°C lower melting temperature. Additionally, the invariant D116 residue is located in the nicotinamide-binding pocket of SIRT6 and plays a direct role in NAD^+ binding (Figure 2E). The corresponding aspartic acid residue in the crystal structure of bacterial Sir2Tm forms a hydrogen bond with the carboxamide amino group of the nicotinamide moiety. Mutation of the aspartic acid residue to an asparagine decreased the catalytic efficiency of Sir2Tm by two orders of magnitude (Avalos et al., 2005). Therefore, as predicted, a mutation of D116 to asparagine led to a similar reduction in SIRT6 activity.

We recently demonstrated that SIRT6 can be directly activated by long-chain fatty acids in vitro (Feldman et al., 2013). To assess the ability of fatty acids to activate these SIRT6 mutants, we analyzed the in vitro deacetylase activity in the presence of myristic acid. WT and SIRT6 mutants were reacted with 50 μM H3K9Ac peptide and 0.5 mM NAD^+ in the presence of 300 μM myristic acid. The fold change in activity of each mutant in the presence of myristic acid was compared to WT. D25N (11 ± 0.5) and E36V (11 ± 2) were activated by myristic acid to the same level as WT SIRT6 (10 ± 1), whereas P274L (7 ± 1) and T263P (6 ± 1) were activated to a slightly lesser extent than WT (Figure 2J). Interestingly, the activity of A89S SIRT6 decreased 2-fold in the presence of myristic acid, which resulted in a 20-fold decrease in activation relative to WT.

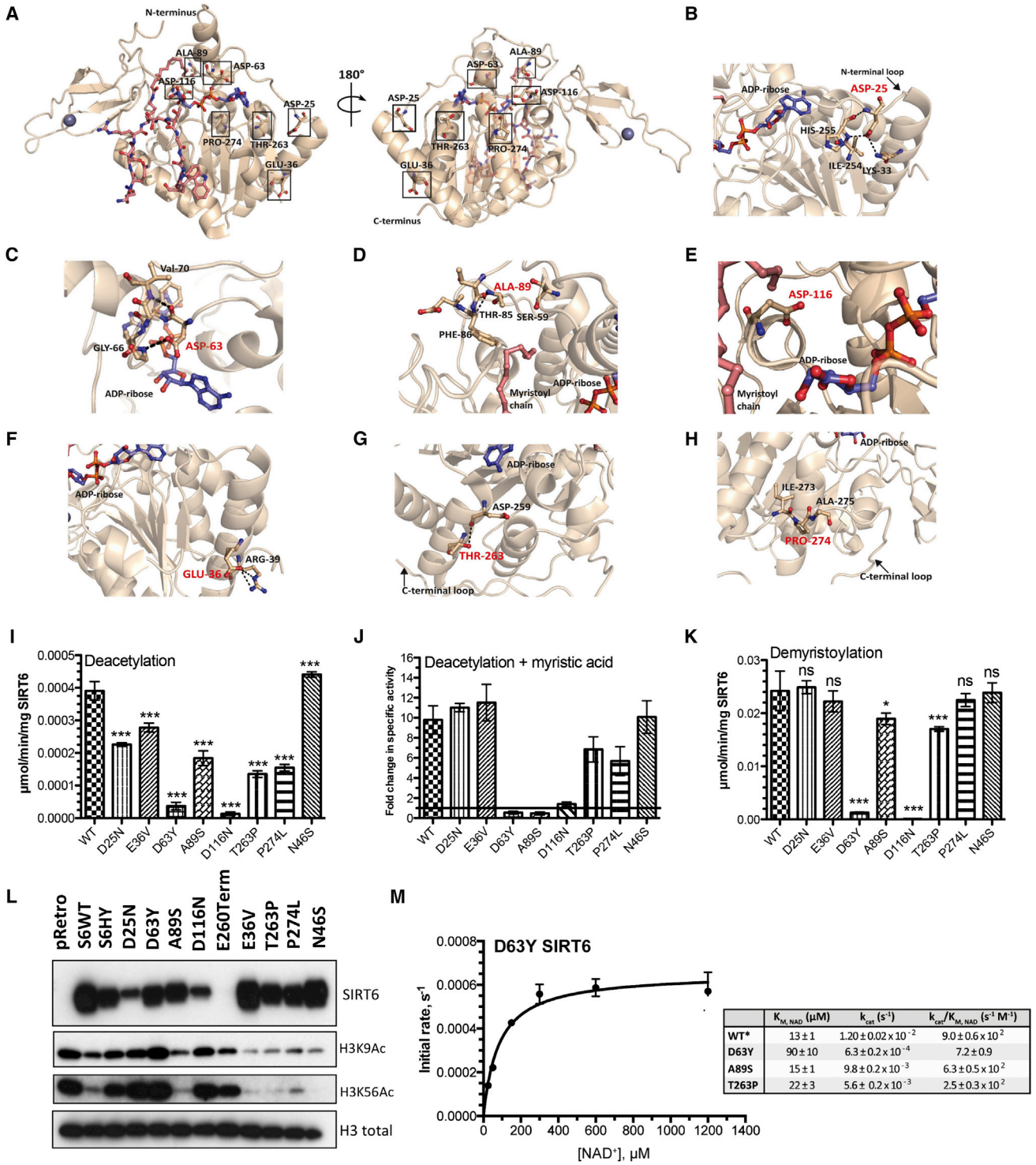

	$K_{M, NAD}$ (µM)	k_{cat} (s^{-1})	$k_{cat}/K_{M, NAD}$ ($s^{-1} M^{-1}$)
WT*	13 ± 1	$1.20 \pm 0.02 \times 10^{-2}$	$9.0 \pm 0.6 \times 10^{2}$
D63Y	90 ± 10	$6.3 \pm 0.2 \times 10^{-4}$	7.2 ± 0.9
A89S	15 ± 1	$9.8 \pm 0.2 \times 10^{-3}$	$6.3 \pm 0.5 \times 10^{2}$
T263P	22 ± 3	$5.6 \pm 0.2 \times 10^{-3}$	$2.5 \pm 0.3 \times 10^{2}$

Figure 2. Structural and Enzymatic Analysis of WT SIRT6 and SIRT6 Point Mutations

(A) Locations of mutated residues mapped on the crystal structure of SIRT6 (PDB: 3GZ6).

(B–H) Zoomed-in view of the mutated residues highlighted in red. Also displayed are residues in close proximity to the mutated residues and hydrogen bonding interactions.

(I) SIRT6 deacetylase activity measured in vitro. Recombinant WT and SIRT6 mutants (2 µM) were incubated with 50 µM H3K9Ac peptide and 0.5 mM NAD^+.

(J) Fold change in SIRT6-dependent deacetylation in the presence of 300 µM myristic acid.

(legend continued on next page)

To determine whether cancer-associated mutations in SIRT6 affect the previously reported demyristoylase activity (Jiang et al., 2013), WT and SIRT6 mutants were reacted with 50 μM H3K9Myr peptide in the presence of 0.5 mM NAD^+ and analyzed as described above. As predicted, the N46S variant, which was used as a control in the assay, displayed demyristoylase activity equal to WT. Surprisingly, the D25N, E36V, A89S, and P274L mutations displayed similar ability to remove myristoyl groups compared with WT SIRT6 (≥75%). The demyristoylase activity of T263P activity was greater than 70% of WT, whereas D63Y and D116N were the only two mutants that exhibited less than 5% demyristoylase activity (Figure 2K), which is consistent with loss of general catalytic function. Importantly, these data suggest that cancer-associated point mutations may specifically inactivate SIRT6 deacetylase activity without affecting its ability to remove larger fatty acyl groups. Most dramatic is the A89S mutant, which displays similar demyristoylation activity to that of WT but cannot be activated toward acetylated histone substrates (compare Figures 2J and 2K).

To examine the effect of SIRT6 mutations on histone acetylation in vivo, we analyzed total H3K9 and H3K56 acetylation levels in bulk chromatin of MEFs following short-term expression of either WT or mutant SIRT6 using a dox-inducible system. In this context, the D25N, D63Y, D116N, and E260Term mutants failed to reduce levels of H3K56 and K9 acetylation when compared to WT SIRT6 (Figure 2L). This is consistent with the reduced deacetylase activity of the D25N and D63Y mutations and the reduced binding of the D116N and E260Term mutants to chromatin. The D25N mutant behaves similarly to a previously described, catalytically inactive mutation where the highly conserved histidine 133, within the core sirtuin domain of SIRT6, is mutated to tyrosine (H133Y; Mostoslavsky et al., 2006). The SIRT6 mutants E36V, A89S, T263P, and P274L were able to reduce the levels of acetylated H3K56 and H3K9 in bulk chromatin when overexpressed, despite having decreased in vitro catalytic activity relative to WT (compare Figures 2I and 2L), suggesting that overexpression can overcome their reduced enzymatic activity. However, these changes in bulk chromatin may not specifically reflect the effect of these SIRT6 mutants to deacetylate histones in the promoter regions of specific SIRT6-regulated genes.

The D63Y mutant displays limited deacetylase and demyristoylase activity and led to large increases in acetylation in vivo. As described earlier, D63 is located in the NAD^+-binding pocket and is 3 Å from the adenosine moiety of NAD^+ (Figure 2C). To test the hypothesis that D63Y decreases the affinity of SIRT6 for NAD^+, we performed steady-state kinetic analysis with increasing NAD^+ at saturating levels of H3K9Myr peptide. The H3K9Myr peptide was used in the assay due to the prohibitively high concentration of H3K9Ac peptide required for saturation (estimated at nearly 4.5 mM; Feldman et al., 2013). The data were subjected to Michaelis-Menten analysis, and the kinetic constants were compared to WT SIRT6, as well as to A89S and T263P, which were expected to show no defects in NAD^+ affinity (Figures 2M and S1E). The k_{cat}/K_m value is the lowest for D63Y ($7.2 \pm 0.9\ s^{-1}\ M^{-1}$) and is 125 times less efficient than WT SIRT6 ($9.0 \pm 0.6 \times 10^2\ s^{-1}\ M^{-1}$). Whereas the small decrease in the catalytic efficiency of A89S ($6.3 \pm 0.5 \times 10^2\ s^{-1}\ M^{-1}$) and T263P ($2.5 \pm 0.3 \times 10^2\ s^{-1}\ M^{-1}$) is caused by a decrease in the k_{cat}, the decrease in D63Y is due to both a decrease in k_{cat} and an increase in the K_m for NAD^+. The K_m for NAD^+ increased approximately seven times (90 ± 10 μM versus 13 ± 1 μM), and the k_{cat} decreased ~19 times relative to WT SIRT6 ($6.3 \pm 0.2 \times 10^{-4}\ s^{-1}\ M^{-1}$ versus $1.20 \pm 0.02 \times 10^{-2}\ s^{-1}\ M^{-1}$). Together, the results indicate a mutation of D63 to tyrosine disrupts both the affinity of SIRT6 for NAD^+ and catalysis, leading to dramatic loss of SIRT6-dependent deacetylation and the subsequent robust increase in acetylation observed in vivo.

SIRT6 Mutants Fail to Repress Glycolytic Genes

We next determined the ability of the mutants to repress HIF1α and MYC transcriptional activity. As shown in Figures 3A and 3B, both HIF1α and MYC luciferase reporters were repressed by WT SIRT6; however, the mutants were unable to repress either HIF1α or MYC luciferase activity. We next expressed each of these mutants as well as WT SIRT6 in SIRT6 KO MEFs. Consistent with their inability to repress HIF1a and MYC transcriptional activity, the SIRT6 mutants were unable to decrease glucose uptake by SIRT6 KO MEFs (Figure 3C). Similarly, these mutants were unable to repress the glycolytic genes *pfkm*, *pdk1*, and *ldhb* (Figure 3D) and the ribosomal genes *rpl3*, *rpl23*, and *rps15a* (Figure S2B). Interestingly, E36V, T263P, and P274L were still able to partially inhibit glucose uptake. Thus, we tested additional genes that may explain why these SIRT6 mutants may be able to repress glucose uptake and found that, unlike other glycolysis-related genes, these mutants retain the ability to silence the glucose transporter 1 (*glut1*), a SIRT6 target gene that is directly responsible for controlling glucose uptake (Figure S2A). Taken together, these results suggest that these cancer-associated SIRT6 mutations are unable to repress MYC- and HIF1α-dependent transcription.

To further explore the mechanism by which SIRT6 regulates glycolytic gene expression, we performed chromatin immunoprecipitation (ChIP) for H3K9Ac, H3K56Ac, and SIRT6 in cells expressing SIRT6 WT and mutant alleles H133Y, D63Y, A89S, and D116N. We found that WT SIRT6 binds to *pdk1*, *glut1*, *ldha*, and *ldhb* and is able to deacetylate H3K56, as previously reported (Figures 3E and 3F; Zhong et al., 2010), thus leading to the reduced gene expression we observed in Figure 3D. The SIRT6 mutants D63Y and A89S were able to bind to the

(K) SIRT6 demyristoylase activity measured in vitro. WT and SIRT6 mutants (0.5 μM) were incubated with 50 μM H3K9Myr peptide and 0.5 mM NAD^+ (I–K; $n \geq 3$; ±SD; $^{**}p \leq 0.01$; $^{***}p \leq 0.001$; ns, $p > 0.05$).

(L) Western blot of chromatin fraction in SIRT6 KO MEFs with doxycycline-inducible overexpression of WT SIRT6 and SIRT6 mutants. SIRT6 and H3 total western blots from Figure 1C are represented here for direct comparison.

(M) Steady-state rates of demyristoylation were measured by varying NAD^+ (25–1,200 μM) in the presence of 0.5 μM D63Y SIRT6 and 50 μM H3K9Myr peptide. Calculated values determined from non-linear regression fits to Michaelis-Menten are shown below for WT, D63Y, A89S, and T263P ($n \geq 3$; ±SD). *WT SIRT6 values previously published (Feldman et al., 2015).

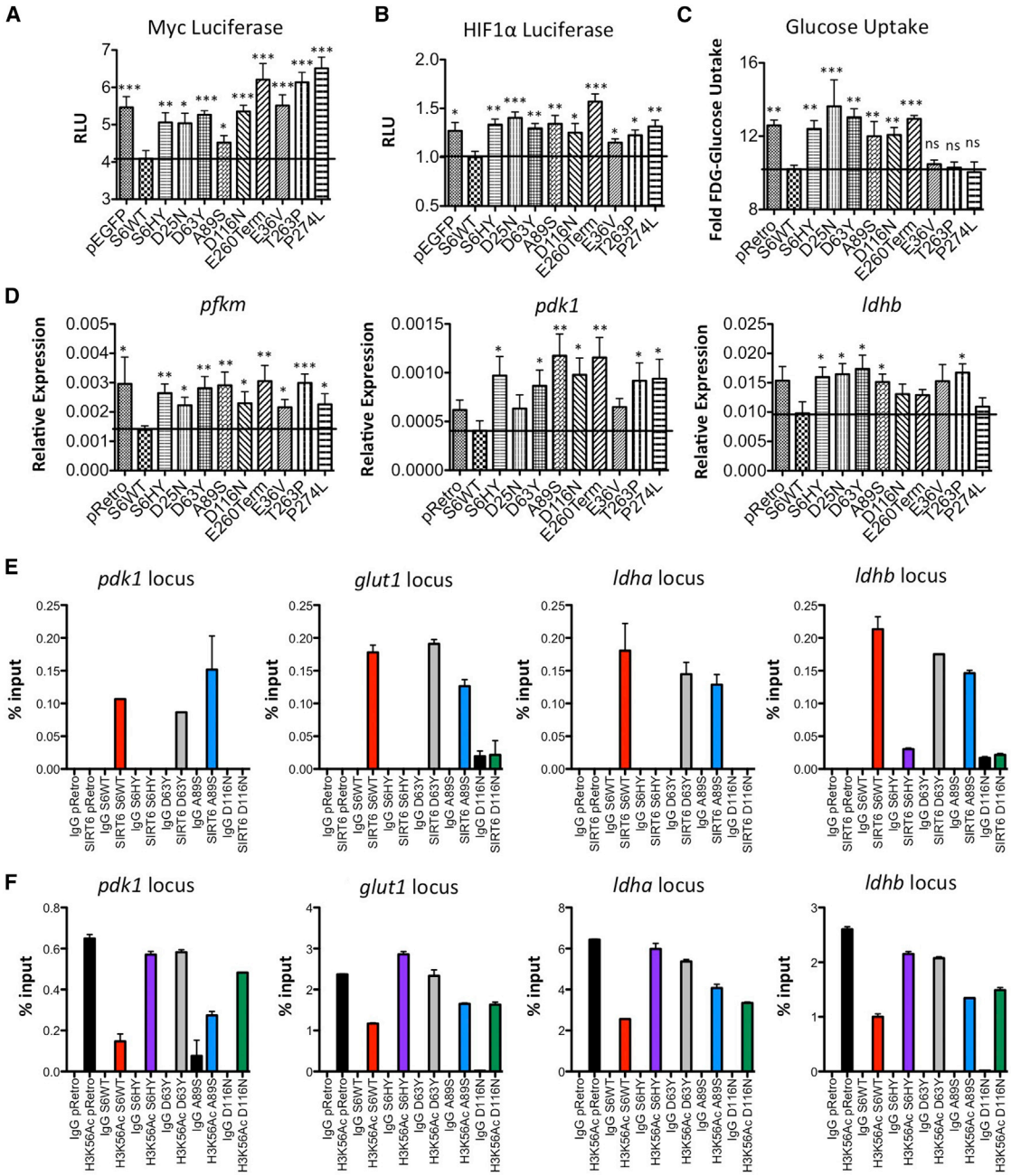

Figure 3. SIRT6 Cancer-Associated Point Mutations Fail to Repress HIF and MYC

(A and B) Luciferase reporter gene assay for MYC (A) and HIF1α (B) in 293T cells transiently expressing the indicated SIRT6 constructs. Data are shown as mean ± SEM between triplicates and are representative of four independent experiments.

(C) NBDG-glucose uptake in SIRT6 KO MEFs. Data are shown as mean ± SEM between duplicates and are representative of two independent experiments.

(D) Quantitative real-time PCR showing the expression of indicated genes. Data are shown as mean ± SEM between duplicates in six independent experiments.

(E and F) Chromatin immunoprecipitation for SIRT6 (E) and H3K56Ac (F) in SIRT6 KO MEFs expressing the indicated SIRT6 constructs followed by qPCR amplification of the indicated glycolytic genes. Data are shown as mean ± SEM between duplicates.

*$p \leq 0.05$; **$p \leq 0.01$; ***$p \leq 0.001$.

glycolytic genes, whereas D116N was unable to bind, most likely due to its reduced protein stability (Figure 3E). Similar to our previous in vitro and cellular characterization data, H133Y, D63Y, A89S, and D116N were unable to deacetylate H3K56 to the same degree as WT SIRT6 (Figure 3F). Interestingly, we also observed that expression of WT SIRT6 had a less-dramatic impact on H3K9Ac levels both in bulk chromatin (Figure 2L) and over the promoters of specific SIRT6 target genes

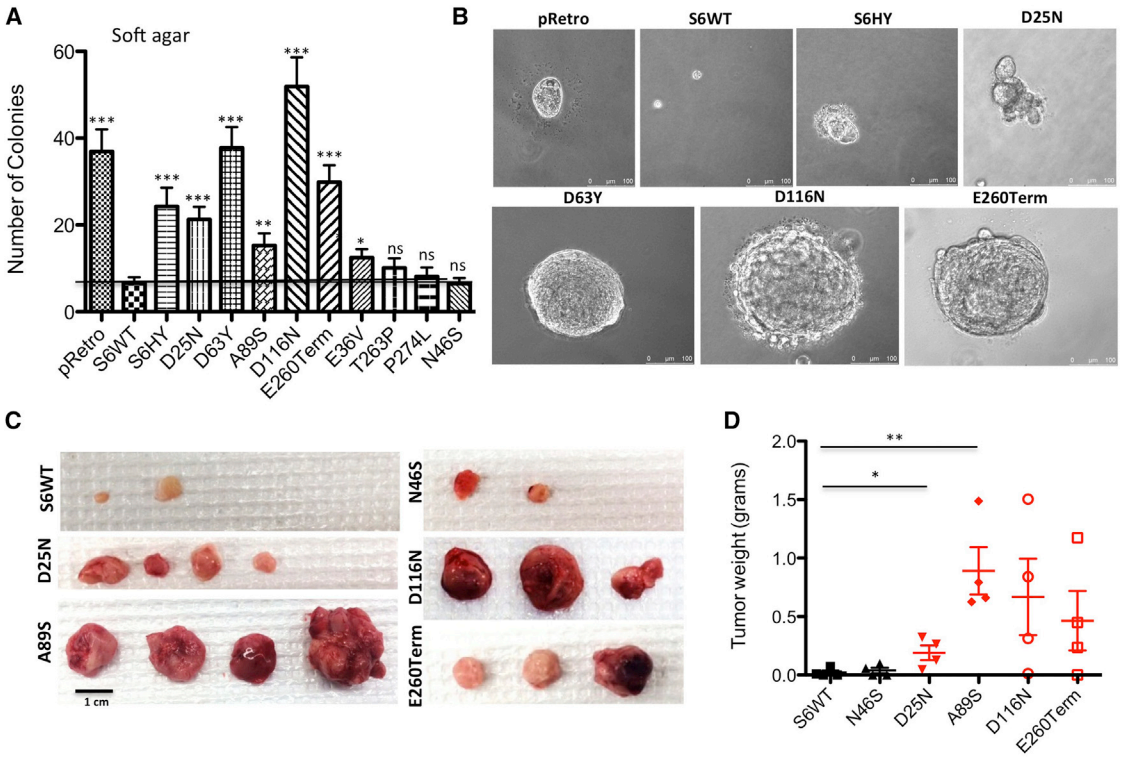

Figure 4. SIRT6 Cancer-Associated Point Mutations Fail to Repress Anchorage-Independent Growth

(A) Quantification of colonies grown in soft agar of SIRT6 KO MEFs expressing each mutant. Data are shown as mean ± SEM between triplicates in four independent experiments.

(B) Representative pictomicrographs of colonies.

(C) Gross images of subcutaneous tumors grown in SCID mice of SIRT6 KO cells re-expressing the indicated SIRT6 constructs (n = 5).

(D) Quantification of tumor weight from (C).

*p ≤ 0.05; **p ≤ 0.01; ***p ≤ 0.001.

(Figure S2C), suggesting that removal of H3K56Ac marks may be more critical for SIRT6-mediated gene repression in this system.

SIRT6 Mutants Fail to Suppress Anchorage-Independent Growth and Tumor Formation

To assess the ability of these SIRT6 mutants to repress transformation, we first performed soft agar colony-formation assays on our SIRT6 KO MEFs engineered to express either empty vector, WT SIRT6, or each of our cancer-associated mutations. Indeed, we found that all of the tumor-associated mutations were unable to suppress colony formation in soft agar to the same degree as WT SIRT6 (Figures 4A and 4B). The only exceptions were T263P and P274L, consistent with their ability to suppress glucose uptake, indicating that overexpression of either mutant may be sufficient to overcome its reduced enzymatic activity. Thus, the histone deacetylase activity of SIRT6 seems critical to suppress cellular transformation. To test these mutants in a more stringent environment, we implanted D25N, A89S, D116N, E260Term, the variant N46S, and WT SIRT6 subcutaneously into the flanks of SCID mice and monitored tumor growth over 2 months. Strikingly, the cells expressing the different mutants readily formed tumors, whereas cells re-expressing WT SIRT6 and the variant N46S formed negligible tumors (Figures 4C and 4D). These results indicate that these specific mutations eliminate the capacity of SIRT6 to protect against tumor formation in vivo.

DISCUSSION

Using data mining from The Cancer Genome Atlas (TCGA), we identified eight point mutations in SIRT6, which spontaneously arose in a variety of human cancers. Based on biochemical, biological, and structural analysis, we find that these mutations render the protein unable to fully repress HIF1α and MYC transcriptional activity, resulting in a glycolytic switch and cellular transformation. Importantly, several of these mutations decrease SIRT6 deacetylase activity while maintaining the ability to remove myristoyl groups, demonstrating that SIRT6 deacetylase activity, as opposed to the demyristoylase activity, is critical for its major tumor-suppressor functions (Table S1). Thus, although rare, point mutations in SIRT6 are selected for in human cancers, further highlighting SIRT6 as a tumor suppressor and its molecular function as a histone deacetylase repressing both pro-growth and glycolytic phenotypes.

From a genetic perspective, tumor suppressors, in contrast to oncogenes, are frequently deleted, silenced, and, less often,

mutated (Vogelstein et al., 2013). Although in previous work, we identified deletion and transcriptional silencing of SIRT6 as mechanisms through which tumors eliminate or reduce SIRT6 activity, in this study, we aimed to identify whether specific point mutations in SIRT6 could provide tumors with a selective growth advantage. Also, such precise mutations might provide the opportunity to determine which catalytic activity of SIRT6 is the main driver of tumor suppression, as sirtuins are now recognized as general protein deacylases (Feldman et al., 2013). Strikingly, each one of the cancer-associated mutations we identified clearly reduced SIRT6 function, either by affecting SIRT6 protein stability or catalytic activity.

The mutations were distributed broadly throughout the gene, suggesting that, likely, no particular hot spots evolved that selectively affect SIRT6 activity. When analyzed for protein stability, two specific mutations (D116N and E260Term) exhibited less chromatin binding and protein levels, despite normal RNA expression. E260Term was the only mutation that lacked nuclear staining, consistent with a deletion of the nuclear localization signal in this mutant. D116N, in turn, appears to directly affect stability of the protein, as confirmed by a strong decrease in melting temperature compare to WT SIRT6. At physiologic temperatures, this protein will mostly remain unfolded and be subjected to degradation. All the other mutations affected SIRT6 catalytic activity. D63Y significantly affects NAD^+ binding, whereas D25N, E36V, A89S, T263P, and P274L mutations are not directly involved in binding the acetylated substrate or NAD^+ and likely decrease SIRT6 activity by imposing specific structural defects that alter the deacetylase function.

The SIRT6 A89S mutant is especially intriguing given that it exhibits deacetylase activity that is approximately 50% of WT in the absence of activation by myristic acid in our in vitro assays. Whereas not dramatically inhibiting basal in vitro deacetylase activity of SIRT6, the A89S mutation prevents SIRT6 from reaching maximal activity level in the presence of free fatty acid. A89 is located on a loop in the back of the active site and forms a backbone hydrogen-bonding interaction with T85 in the loop (Figure 2D). Thus, mutation of A89 to a serine likely alters the orientation of the loop, disfavoring myristic acid binding. In this context, the activity of the A89S mutant is comparable with the D116N mutant. Therefore, we propose that both basal and enhanced (i.e., with free fatty acid) activity of SIRT6 may be important for its tumor-suppressive effects. The A89S mutant reduces the levels of H3K9Ac and H3K56Ac in bulk chromatin similar to WT SIRT6. However, when looking at specific SIRT6 target genes, the A89S mutant is defective in removing H3K56Ac groups from specific SIRT6 target genes, such as *pdk1*, *glut1*, *ldha*, and *ldhb*. Additionally, the A89S mutation displays a more-pronounced effect on tumor growth in vivo compared to its ability to form colonies in soft agar. This may reflect the inability of the A89S mutant to be activated by free fatty acids or a functionally related small molecule that is present in vivo, but not in vitro.

Interestingly, ChIP analysis revealed that SIRT6 deacetylated H3K56Ac more efficiently than H3K9Ac at the promoters of glycolytic genes. This is suggestive of a role for H3K56Ac in gene silencing, consistent with our previous publication (Sebastián et al., 2012). It is also important to note that we cannot completely rule out that some of the phenotypes observed could be due to the possibility that these mutations affect the binding of SIRT6 with other yet to be described partners, thus influencing their regulation and function. Finally, whereas all cancer-associated mutations had decreased deacetylase activity, the N46S variant found in the human population displayed WT level activity, providing additional evidence these mutations were specifically selected for in these cancers.

Recent studies identified a de-fatty acylase activity for SIRT6, by virtue of its capacity to modulate TNFα secretion by removing a myristoyl group (Jiang et al., 2013). This recently characterized activity has created mechanistic uncertainty as to whether SIRT6 functions predominantly as a long-chain deacylase or as a H3K9 and H3K56 deacetylase in order to regulate cellular activity. Notably, all the cancer mutants exhibit clear defective histone deacetylation activity, whereas their demyristoylase activity was similar to the WT enzyme, with the exception of D63Y and D116N, which affect NAD^+ binding. Additionally, ADP-ribosylation activity has also been ascribed to SIRT6. However, consistent with published reports (Du et al., 2009; Feldman et al., 2012; Tanner et al., 2000), we were unable to detect significant evidence of any ADP-ribosylation activity by WT SIRT6 or any of the mutants we tested (data not shown), suggesting that such activity for SIRT6 may only be observed under specific circumstances (Mao et al., 2011). These results indicate that histone deacetylation is the main activity conferring tumor-suppressive functions to SIRT6, likely through its ability to repress glycolytic and ribosomal protein gene expression, as we previously published (Sebastián et al., 2012).

Taken together, our results provide convincing mechanistic evidence for a tumor-suppressive role for this enzyme and increase our understanding of the interplay between epigenetics, metabolism, and cancer.

EXPERIMENTAL PROCEDURES

Cell Lines

SIRT6 KO primary MEFs were generated from 13.5-day-old embryos as described (Mostoslavsky et al., 2006). These cells were immortalized by using the standard 3T3 protocol. Please see Supplemental Experimental Procedures for culture conditions.

Computational Analysis to Identify SIRT6 Mutations

Somatic mutations in SIRT6 were obtained from Lawrence et al. (2014), which are available at http://www.tumorportal.org. Details on discovery of somatic mutations are found in Lawrence et al. (2014).

Expression and Purification of Recombinant Human SIRT6

His-tagged WT and mutant SIRT6 proteins were overexpressed in BL21(DE3) *E. coli* strain, as previously described (Feldman et al., 2015). Cells were harvested by centrifugation and stored at −80°C. SIRT6 WT and mutant proteins were purified by nickel affinity resin chromatography as reported previously (Pan et al., 2011). Protein concentrations were determined by the Bradford reagent assay.

Gel Electrophoresis and Western Blotting

Chromatin fractions and western blot analysis was performed as previously described (Sebastián et al., 2012); details are listed in Supplemental Experimental Procedures. Antibodies used were anti-SIRT6 (Abcam; ab62739),

anti-H3K9Ac (Millipore 07-352), anti-H3K56Ac (ab76307), anti-GFP (ab290), or total-H3 (ab1791) as a loading control.

Immunofluorescence

293T cells were transfected using Trans-IT 293 (Mirus) with empty vector, pEGFP-SIRT6, or the SIRT6 mutant constructs. Twenty-four hours after transfection, cells were trypsinized and seeded onto 8-well chamber slides and allowed to adhere overnight. Cells were then fixed using a 2% paraformaldehyde in a 1% PBS solution, permeabilized with 0.1% sodium citrate and 0.1% Triton X-100, and nuclei were stained using DAPI. Images were taken using a fluorescent microscope.

Statistics

For steady-state deacylation assays, real-time RT-PCR analysis, glucose uptake, luciferase reporter assay, ChIP assay, anchorage-independent growth, and tumor size, significance was analyzed using two-tailed Student's t test. A p value of less than 0.05 was considered statistically significant.

Thermal Denaturation Assays

Thermal denaturation assays were performed to determine the melting temperature (T_m) of WT, D25N, D63Y, and D116N SIRT6. Purified proteins were diluted to 10 μM (20 mM sodium phosphate [pH 7.5]) containing 3.75× Sypro Orange (Invitrogen; delivered at 5,000×). Samples (35 μl) were aliquoted into PCR strip tubes and placed in a Bio-Rad CFX96 Real-Time System C1000 thermal cycler. The temperature was increased at a rate of 0.5°C/min over a range of 10°C–95°C, and fluorescence was monitored with the FRET channels. At least three trials were performed for each SIRT6 variant. The measured fluorescence was normalized so that the minimum fluorescence was set to 0 and the maximum fluorescence set to 1. The data were fitted to Equation 1 as previously utilized by Albaugh et al. (2011) to obtain the T_m,

$$I = \left(\frac{1}{1 + e^{(T_m - T)/C}}\right), \qquad \text{(Equation 1)}$$

where I is the normalized fluorescence value at temperature T and C is a slope factor.

HPLC Deacylation Assay

Peptides corresponding to residues 4–17 of histone H3 (acetyl: AcQTARKac STGGKAPR-WW-NH_2 and myristoyl: Ac-QTARKmyrSTGGKAPRWW-NH_2) were synthesized as described previously (Feldman et al., 2013). Deacylation reactions were analyzed by reversed phase high-performance liquid chromatography on Kinetex C18 column (100 Å; 100 × 4.6 mm; 2.6 μm; Phenomenex) by monitoring the formation of the deacylated product at 214 nm (Feldman et al., 2013) and also described in Supplemental Experimental Procedures.

Steady-State Kinetic Analyses

Steady-state rates were measured by varying NAD^+ (2–1,200 μM) in the presence of 0.5 μM WT, D63Y, A89S, or T263P SIRT6 and 50 μM NAD^+ in 20 mM sodium phosphate (pH 7.5) at 37°C. Initial velocities were determined and data were fitted to the Michaelis-Menten equation.

Glucose Uptake Assay

Cells were grown under normal conditions for 24 hr, and 100 μM 2-NBDG (Invitrogen) was added to the media for 2 hr. Fluorescence was measured by flow cytometry using a FACSCalibur Analyzer (BD).

Luciferase Reporter Assay

MYC and HIF1α transcriptional activity was determined in 293T cells using pMYC-luc and mpGL3:HRE4 constructs, respectively, by luciferase reporter assay as previously described (Sebastián et al., 2012; Zhong et al., 2010); details are listed in Supplemental Experimental Procedures.

Real-Time RT-PCR Analysis

Total RNA was extracted with the TriPure Isolation Reagent (Roche) as described by the manufacturer. For cDNA synthesis, 1 μg of total RNA was reverse transcribed by using the QuantiTect Reverse Transcription Kit (QIAGEN). Real-time PCR was performed as previously described (Sebastián et al., 2012); details are listed in Supplemental Experimental Procedures. Data were expressed as relative mRNA levels normalized to the β-actin expression level in each sample. The primer sequences are listed in Table S2.

ChIP Assays

ChIP assays were performed as previously described (Sebastián et al., 2008), with some modifications; details are listed in Supplemental Experimental Procedures. Antibodies used are 5 μl anti-SIRT6 (Abcam; ab62739), 5 μl anti-H3K9Ac (Millipore 07-352), and 5 μl anti-H3K56Ac (ab76307). A control was performed with unspecific IgGs (AbCam). Real-time RT-PCR was performed with primers listed in Table S2.

Anchorage-Independent Growth

Five thousand cells were resuspended in 0.4% agar and plated in triplicates in 6-well plates containing a 0.8% base agar layer. Colonies were grown in the presence of doxycycline for 3 months and counted. Media was changed every 3 days.

Xenografts

4×10^6 cells in 100 μl of 50% Matrigel were injected subcutaneously into the flanks of SCID mice (n = 5; Taconic Farms) that were maintained on doxycycline (200 μg/ml) in their drinking water. Mice were checked for the appearance of tumors twice a week, and the tumors were harvested when they reached ~100 mm^3 in size. These experiments were approved by the IACUC Committee of MGH, protocol number 2007N000200.

SUPPLEMENTAL INFORMATION

Supplemental Information includes Supplemental Experimental Procedures, two figures, and two tables and can be found with this article online at http://dx.doi.org/10.1016/j.celrep.2015.09.022.

AUTHOR CONTRIBUTIONS

S.K., J.L.F., M.A.K., S.D., and A.R.C. collected the data. S.K., J.L.F., and M.A.K. analyzed the data. R.M., D.M.S., C.S., and J.M.D. contributed to the experimental design. C.M. and G.G. performed computational analysis to identify SIRT6 mutations. S.K., J.L.F., J.M.D., and R.M. wrote the paper. All authors discussed the results and commented on the manuscript.

ACKNOWLEDGMENTS

We thank members of the R.M. and J.M.D. labs for invaluable discussions and advice. This work was supported in part by NIH grants 1R01CA175727-01A1, DK088190-01A1 (to R.M.), and NIH GM065386 (to J.M.D). R.M. is the Kristine and Bob Higgins MGH Research Scholar, the Warshaw Institute Fellow, and a Howard Goodman Awardee. S.K. is the recipient of a Canadian Institutes of Health Research postdoctoral fellowship. C.S. is supported by the Visionary postdoctoral fellowship from the Department of Defense.

Received: May 19, 2015
Revised: July 30, 2015
Accepted: September 8, 2015
Published: October 8, 2015

REFERENCES

Albaugh, B.N., Arnold, K.M., Lee, S., and Denu, J.M. (2011). Autoacetylation of the histone acetyltransferase Rtt109. J. Biol. Chem. *286*, 24694–24701.

Avalos, J.L., Bever, K.M., and Wolberger, C. (2005). Mechanism of sirtuin inhibition by nicotinamide: altering the NAD(+) cosubstrate specificity of a Sir2 enzyme. Mol. Cell *17*, 855–868.

Du, J., Jiang, H., and Lin, H. (2009). Investigating the ADP-ribosyltransferase activity of sirtuins with NAD analogues and 32P-NAD. Biochemistry *48*, 2878–2890.

Feldman, J.L., Dittenhafer-Reed, K.E., and Denu, J.M. (2012). Sirtuin catalysis and regulation. J. Biol. Chem. *287*, 42419–42427.

Feldman, J.L., Baeza, J., and Denu, J.M. (2013). Activation of the protein deacetylase SIRT6 by long-chain fatty acids and widespread deacylation by mammalian sirtuins. J. Biol. Chem. *288*, 31350–31356.

Feldman, J.L., Dittenhafer-Reed, K.E., Kudo, N., Thelen, J.N., Ito, A., Yoshida, M., and Denu, J.M. (2015). Kinetic and Structural Basis for Acyl-Group Selectivity and NAD(+) Dependence in Sirtuin-Catalyzed Deacylation. Biochemistry *54*, 3037–3050.

Gil, R., Barth, S., Kanfi, Y., and Cohen, H.Y. (2013). SIRT6 exhibits nucleosome-dependent deacetylase activity. Nucleic Acids Res. *41*, 8537–8545.

Jiang, H., Khan, S., Wang, Y., Charron, G., He, B., Sebastian, C., Du, J., Kim, R., Ge, E., Mostoslavsky, R., et al. (2013). SIRT6 regulates TNF-α secretion through hydrolysis of long-chain fatty acyl lysine. Nature *496*, 110–113.

Kawahara, T.L., Michishita, E., Adler, A.S., Damian, M., Berber, E., Lin, M., McCord, R.A., Ongaigui, K.C., Boxer, L.D., Chang, H.Y., and Chua, K.F. (2009). SIRT6 links histone H3 lysine 9 deacetylation to NF-kappaB-dependent gene expression and organismal life span. Cell *136*, 62–74.

Lawrence, M.S., Stojanov, P., Mermel, C.H., Robinson, J.T., Garraway, L.A., Golub, T.R., Meyerson, M., Gabriel, S.B., Lander, E.S., and Getz, G. (2014). Discovery and saturation analysis of cancer genes across 21 tumour types. Nature *505*, 495–501.

Mao, Z., Hine, C., Tian, X., Van Meter, M., Au, M., Vaidya, A., Seluanov, A., and Gorbunova, V. (2011). SIRT6 promotes DNA repair under stress by activating PARP1. Science *332*, 1443–1446.

Michishita, E., McCord, R.A., Berber, E., Kioi, M., Padilla-Nash, H., Damian, M., Cheung, P., Kusumoto, R., Kawahara, T.L., Barrett, J.C., et al. (2008). SIRT6 is a histone H3 lysine 9 deacetylase that modulates telomeric chromatin. Nature *452*, 492–496.

Mostoslavsky, R., Chua, K.F., Lombard, D.B., Pang, W.W., Fischer, M.R., Gellon, L., Liu, P., Mostoslavsky, G., Franco, S., Murphy, M.M., et al. (2006). Genomic instability and aging-like phenotype in the absence of mammalian SIRT6. Cell *124*, 315–329.

Pan, P.W., Feldman, J.L., Devries, M.K., Dong, A., Edwards, A.M., and Denu, J.M. (2011). Structure and biochemical functions of SIRT6. J. Biol. Chem. *286*, 14575–14587.

Sebastián, C., Serra, M., Yeramian, A., Serrat, N., Lloberas, J., and Celada, A. (2008). Deacetylase activity is required for STAT5-dependent GM-CSF functional activity in macrophages and differentiation to dendritic cells. J. Immunol. *180*, 5898–5906.

Sebastián, C., Zwaans, B.M., Silberman, D.M., Gymrek, M., Goren, A., Zhong, L., Ram, O., Truelove, J., Guimaraes, A.R., Toiber, D., et al. (2012). The histone deacetylase SIRT6 is a tumor suppressor that controls cancer metabolism. Cell *151*, 1185–1199.

Tanner, K.G., Landry, J., Sternglanz, R., and Denu, J.M. (2000). Silent information regulator 2 family of NAD- dependent histone/protein deacetylases generates a unique product, 1-O-acetyl-ADP-ribose. Proc. Natl. Acad. Sci. USA *97*, 14178–14182.

Tennen, R.I., Berber, E., and Chua, K.F. (2010). Functional dissection of SIRT6: identification of domains that regulate histone deacetylase activity and chromatin localization. Mech. Ageing Dev. *131*, 185–192.

Vogelstein, B., Papadopoulos, N., Velculescu, V.E., Zhou, S., Diaz, L.A., Jr., and Kinzler, K.W. (2013). Cancer genome landscapes. Science *339*, 1546–1558.

Warburg, O. (1956). On the origin of cancer cells. Science *123*, 309–314.

Zhong, L., D'Urso, A., Toiber, D., Sebastian, C., Henry, R.E., Vadysirisack, D.D., Guimaraes, A., Marinelli, B., Wikstrom, J.D., Nir, T., et al. (2010). The histone deacetylase Sirt6 regulates glucose homeostasis via Hif1alpha. Cell *140*, 280–293.